

## Evidence of Evolutionary Conservation of Function between the Thyroxine Transporter Oatp1c1 and Major Facilitator Superfamily Members

Daniel E. Westholm, Jacob D. Marold, Kevin J. Viken, Alicia H. Duerst, Grant W. Anderson, and Jon N. Rumbley

Department of Pharmacy Practice and Pharmaceutical Sciences (D.E.W., K.J.V., A.H.D., G.W.A., J.N.R.) and College of Pharmacy and Chemistry and Biochemistry (J.D.M., J.N.R.), University of Minnesota-Duluth, Duluth, Minnesota 55812

Organic anion transporting polypeptide 1c1 (Oatp1c1) is a high-affinity  $T_4$  transporter expressed in brain barrier cells. To identify Oatp1c1 amino acid residues critical for  $T_4$  transport, consensus membrane topology was predicted and a three-dimensional Oatp1c1 structure was generated using the known structures of major facilitator superfamily (MFS) transporters, glycerol 3-phosphate transporter, lactose permease, and the multidrug transporter *Escherichia coli* multidrug resistance protein D as templates. A total of nine amino acid mutations were generated based on amino acid conservation, localization to putative transmembrane domains, and side chain functionality. Mutant constructs were transiently transfected into human embryonic kidney 293 cells and assessed for plasma membrane localization and the capacity to transport substrate  $^{125}I$ - $T_4$ . Wild-type Oatp1c1, R601S, P609A, W277A/W278A, W277F/W278F, G399A/G409A, and G399L/G409L were all expressed at the plasma membrane. Wild-type Oatp1c1 and W277F/W278F displayed biphasic  $T_4$  transport kinetics, albeit the mutant did so with an approximately 10-fold increase in high-affinity Michaelis constant. The W277A/W278A mutation abolished Oatp1c1  $T_4$  transport. G399A/G409A and G399V/G409V mutants displayed near wild-type activity in an uptake screen but exhibited diminished  $T_4$  transport activity at high-substrate concentrations, suggesting a substrate binding site collapse or inability to convert between input and output states. Finally, transmembrane domain 11 mutants R601S and P609A displayed partial  $T_4$  transport activity with significantly reduced maximum velocities and higher Michaelis constant. Arg601 is functionally strongly conserved with members of the MFS whose structures and function have been extensively studied. These data provide the experimental foundation for mapping Oatp1c1 substrate binding sites and reveal evolutionary conservation with bacterial MFS transporter members. (*Endocrinology* 151: 0000–0000, 2010)

Organic anion transporting polypeptides (Oatps in rodents, OATPs in humans) are a superfamily of multispecific organic anion membrane transporters (1, 2). The high-affinity  $T_4$  transporter Oatp1c1/OATP1C1 is expressed in brain barrier cells, including blood-brain barrier (BBB) endothelial cells and choroid plexus epithelial cells comprising the blood-cerebral spinal fluid barrier (BCSFB) (3–5). Although numerous Oatps/OATPs are known to transport  $T_4$ , Oatp1c1/OATP1C1 transports  $T_4$

with an affinity more than 2 orders of magnitude greater than other Oatps/OATPs (6). This suggests that the substrate channel has been selectively tuned to facilitate  $T_4$  transport.

A single Oatp/OATP transporter must have a flexible substrate binding site to accept varying chemical structures. Numerous Oatps/OATPs have displayed atypical kinetic properties, suggestive of the presence of multiple substrate binding sites (7) including Oatp1c1 (8). This

ISSN Print 0013-7227 ISSN Online 1945-7170  
Printed in U.S.A.

Copyright © 2010 by The Endocrine Society

doi: 10.1210/en.2010-0640 Received June 7, 2010. Accepted August 30, 2010.

Abbreviations: Arg, Arginine; GlpT, glycerol 3-phosphate transporter; HEK, human embryonic kidney;  $K_m$ , Michaelis constant; LacY, lactose permease; MFS, major facilitator superfamily; Oatp, organic anion transporting polypeptide in rodents; OATP, Oatp in humans; TMD, transmembrane domain; WT, wild type.

transport characteristic must be an inherent property of Oatp/OATP structure. Through the identification and biochemical characterization of amino acids predicted to line the Oatp/OATP substrate channel, the individual amino acids that comprise the different substrate binding sites may also be defined.

Little is known about Oatp/OATP1C1 structure and the amino acids required for substrate recognition. Comparative modeling between OATPs 1B3 and 2B1 and two members of the major facilitator superfamily (MFS) of transport proteins suggest an Oatp/OATP rocker-switch transport mechanism with alternating inward- and outward-facing active site conformations (9–11) and a positive surface potential in the putative substrate channel (10). Most *in silico* work suggests that Oatps/OATPs possess 12-transmembrane domains (TMDs) with cytoplasmic N and C termini (7). High-resolution structures have been generated for three prokaryotic MFS transporters containing 12 TMDs including lactose permease (LacY), multidrug transporter EmrD, and glycerol 3-phosphate transporter (GlpT) (9, 11, 12). In the present study, using homology modeling to GlpT, LacY, and EmrD, we generated a three-dimensional rat Oatp1c1 structure using MODELLER (University of California, San Francisco, San Francisco, CA) and identified a series of amino acids predicted to line the substrate channel and play a role in Oatp1c1 T<sub>4</sub> transport. Through site-directed mutagenesis, we mutated nine amino acids in Oatp1c1 putative TMDs 2, 6, 8, and 11. Using transient expression of mutated Oatp1c1 constructs in human embryonic kidney (HEK) 293 cells, we identified several amino acids critical for Oatp1c1-mediated T<sub>4</sub> transport. Interestingly, several of these amino acids are positionally equivalent to amino acids that also contribute to substrate recognition in bacterial MFS superfamily members. These data support using prokaryotic MFS transporters to model Oatp/OATP1C1 structure and suggest evolutionary conservation of structure and function between prokaryotic and eukaryotic MFS superfamily members.

## Materials and Methods

### Oatp1c1 mutagenesis

Rat Oatp1c1 was cloned into the expression vector pEF-DEST51 as previously described (13). Site-directed mutagenesis was performed on Oatp1c1-pEF-DEST51 using a Stratagene Quik-Change XL site-directed mutagenesis kit according to the manufacturer's instructions (Stratagene, La Jolla, CA). Resulting mutagenized constructs were isolated and sequence verified. Forward sequences for complementary primers generating specific Oatp1c1 amino acid changes (highlighted in underlining) were as follows: D85A, 5'-ccctctctctggtggaataattgccgcgagtttcgaaatgg-gaatctcc-3'; E89A, 5'-gggaataattgatgtagtttcgcgatcggaatct-

cctggtcataacattcg-3'; N92A, 5'-gggaataattgatgtagtttcgaaatggagcgcctctggtcataacattcg-3'; W277A/W278A, 5'-gatccccagtggtcggggcccgtgctctggttacctaataagca-3'; W277F/W278F, 5'-tccccagtggtcggggccccctttttctggttacctaataagcag-3'; G399A/G409A, 5'-gtcattgctctcatcaatattctgcaagtgcccttgctatattc-3'; G399V/G409A, 5'-gtcattggtctcatcaatattctgcaagtgcccttggaatattc-3'; R601S, 5'-ggcatctacaccttagcagtaagtggtttctgcaggaatcccagcc-3'; P609A, 5'-gcagtaagagttctgcaaggaatcccagctgctggtactttggtggttaattcg-3'.

### Cell culture and transfection

All cell-based studies were carried out in HEK293 cells. HEK293 cells were cultured at 37 C in 5% CO<sub>2</sub> with MEM supplemented to contain 10% fetal bovine serum, 1 mM sodium pyruvate, and nonessential amino acids. Mutant function and expression studies were assessed through transient transfection of HEK293 cells using Lipofectamine 2000 according to the manufacturer's instructions (Invitrogen, Carlsbad, CA). Oatp1c1 function and expression were assessed 24 h after transfection. In all studies, plates and coverslips were coated with rat-tail collagen (Sigma, St. Louis, MO, and Life Technologies, Inc., Carlsbad, CA).

### Time course, velocity vs. substrate assays, and determination of kinetic parameters

Cells were plated and transfected as described above. Five hours before the transport assay, culture medium was changed to MEM supplemented with 10% thyroid hormone-stripped fetal bovine serum and 10 mM sodium butyrate. Transport assays including time-course and kinetic assays were performed as described previously (8). Uptake and Eadie-Hofstee curves were fitted and kinetic parameters were determined using nonlinear regression with GraphPad Prism versions 4 and 5 (GraphPad, San Diego, CA).

### Immunocytochemistry

Cells were plated on glass coverslips and transfected as described above. Immunocytochemistry was performed as previously described (13). Briefly, transfected cells were fixed and probed with primary anti-V5 antibodies and secondary rabbit antimouse-fluorescein isothiocyanate antibodies (Jackson ImmunoResearch, West Grove, PA). Images were captured with a Nikon D-Eclipse laser-scanning confocal unit attached to a Nikon TE2000-U inverted microscope using depth-of-field slices ranging from 30 to 60 μM (Nikon Instruments, Melville, NY). Images were converted to readable format using ImageJ software (<http://rsbweb.nih.gov/ij/>, National Institutes of Health, Bethesda, MD).

### Generation of structural models

#### Rat Oatp sequence alignment

Sequence comparisons were performed between rat Oatp1c1 and all known rat Oatps. Rat Oatp sequences were retrieved by BLAST search against the rat genome on NCBI using rat Oatp1c1 as query (<http://blast.ncbi.nlm.nih.gov/blast.cgi>). To compile amino acid conservation data, a multiple sequence alignment was performed between rat Oatp1c1 and other rat Oatps using PROMALS multiple sequence alignment (14). Default parameters were used in the alignment. Amino acid conservation is indicated with respect to membrane topology (see in Fig. 2).

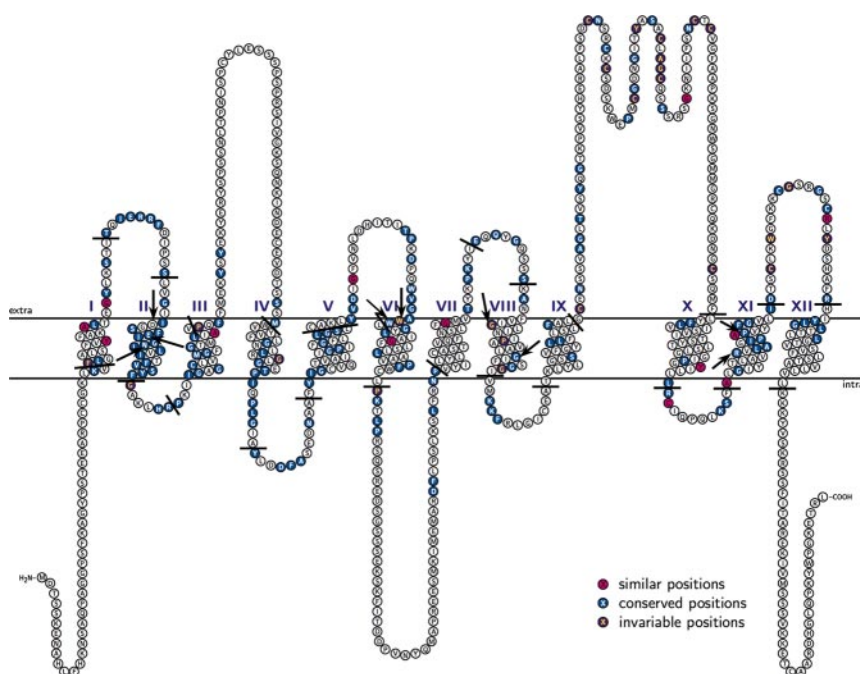


**FIG. 1.** Rat Oatp1c1 membrane topology. Oatp1c1 consensus membrane topology as predicted by rat Oatp protein sequence alignment and the eight predictive algorithms, DAS, BPROMPT, Split4.0, Memstat, HMMTOP2, HMM-TM, Phobius, and PolyPhobias, is shown. The 12 predicted TMDs are located between the two solid lines and numbered with Roman numerals (I–XII). Amino acid conservation among all rat Oatps is mapped onto the Oatp1c1 topology. Red shaded residues denote similar positions (similar side chain character), blue shaded residues denote conserved positions (>50% identity), and purple shaded residues denote invariable positions (100% conservation).

### Generating rat Oatp1c1 consensus membrane topology maps

Oatp1c1 TMDs were first predicted based on a consensus between eight predictive algorithms including DAS, BPROMPT, Split4.0, Memstat, HMMTOP2, HMM-TM, Phobius, and PolyPhobias (15–22) (Supplementary Table 1). Multiple algorithms were used to converge on the most probable spanning regions. The final topology map was then created with TeXtopo (23) using input from sequence conservation information previously determined. Transmembrane predictions for rat Oatp1c1 were validated by sequence comparison to consensus topology predictions with human, chicken, and zebrafish Oatp1c1 (data not shown). This was done by evaluating the coincidence of the predicted transmembrane spans in a multiple sequence alignment between rat, human, chicken, and zebrafish Oatp1c1.

### Alignments between Oatp1c1 and three MFS transporters and generation of three-dimensional Oatp1c1 structure

Structural alignments for the three MFS transporters (GlpT-PDB1PW4, LacY-PDB2V8N, and EmrD-PDB2GFP) were performed using the SAlign feature of MODELLER (24) to produce structural superpositions and sequence alignments of the three transporters. A PROMALS3D alignment was compared with the sequence alignment derived from the structural alignments of the three MFS transporters to evaluate the ability of PROMALS3D to align TMDs of the proteins (25). A rat Oatp1c1 sequence alignment to the three MFS transporters was then produced using PROMALS3D. Rat Oatp1c1 sequences from 1–30, 136–

187, and 451–551 were removed during the alignment because they contained very low homology, and removal resulted in the sequence of more similar length to the MFS transporters. Two poorly aligned TMDs (8 and 12) were manually adjusted to remove gaps at these positions (Supplemental Fig. 1). The optimized sequence alignment was used as input into MODELLER for structure generation using default optimization. Final three-dimensional figures were produced using Chimera [http://www.cgl.ucsf.edu/chimera/; Resource for Biocomputing, Visualization, and Informatics, University of California, San Francisco, San Francisco, CA (26)].

## Results

### Oatp1c1 topology and conservation

The consensus topology of rat Oatp1c1, generated from eight unique programs, is shown in Fig. 1. Supplemental Table 1 shows the predicted domains from each algorithm. The consensus positioning of helices was derived from the mean beginning and ending residue positions from the combined predictions. To

evaluate the robustness of the rat Oatp1c1 helical assignments, a similar prediction was made for the human, chicken, and zebra fish Oatp1c1 sequences. In cases in which variability occurred, a mean of the combined predictions was again used as a correction. Indicated within the topology profile is the sequence conservation across all 16 rat Oatps (Fig. 1). Amino acids targeted for site-directed mutagenesis are identified in the topology map with arrows (Fig. 1).

### Oatp1c1 homology models

In an initial structural alignment of the three bacterial MFS members, GlpT, LacY, and EmrD, the 12 transmembrane helices were nearly superimposable (Supplemental Fig. 2). This was despite the observation that sequence identity from the structure alignment was less than 9% and similarity less than 28% (highest GlpT vs. LacY). A sequence-based alignment using PROMALS3D yielded only slightly improved conservation having less than 16% identity (GlpT vs. EmrD) and less than 35% similarity (GlpT vs. EmrD and GlpT vs. LacP). The structure-based sequence alignment generated in MODELLER, biased toward structural conservation, was used to guide the manual adjustment of the initial alignment of rat Oatp1c1 and the 3 MFS sequences produced in PROMALS3D. Intrahelical gaps in TMDs 8 and 12 were

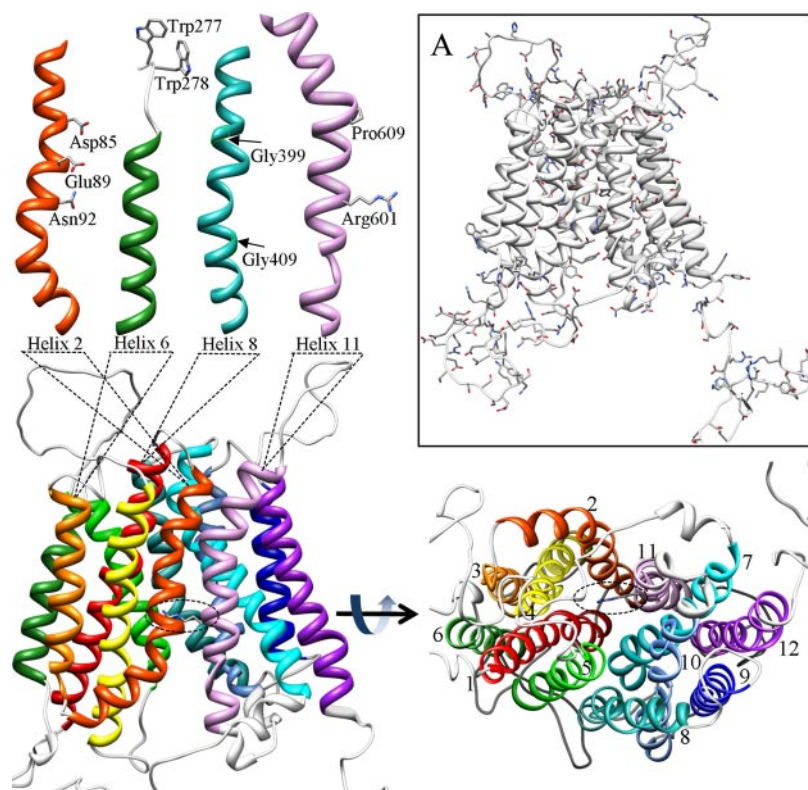


**FIG. 2.** Three-dimensional homology model of Oatp1c1 structure. Oatp1c1 side view with isolated helices showing residues targeted for mutagenesis (*left panel*), and view looking down substrate channel from extracellular side of Oatp1c1 (*right panel*). The *dashed oval* in both *left and right panels* surrounds the exposed R601 residue. TMDs are numbered 1–12. *Inset A* shows the location of all polar amino acids in the current Oatp1c1 homology model.

removed across all of the sequences in the alignment. In addition, rat Oatp1c1 non-TMD residues 1–30, 136–187, and 451–551 were removed during the alignment because they had no structural equivalent in the bacterial MFS proteins. With these changes, three Oatp1c1 structures were generated by homology. The model best satisfying the objective function and having the lowest root mean squared distance between fit atoms across all of the structure was selected for use here (Fig. 2). As would be predicted for membrane proteins and as a measure of reliability, polar and charged amino acids were only oriented toward the substrate pore away from the lipid bilayer (Fig. 2, *inset A*). A structural alignment of all four structures is given in Supplemental Fig. 2. Low identity in the extra- and intracellular domains did not allow modeling of the loops between TMDs. The homology modeled helices always include the regions predicted by consensus prediction but are generally extended in length. This model of Oatp1c1 shows an even stronger bias of amino acid conservation to the membrane spans (Fig. 1). An important outcome of the homology modeling, not apparent in early sequence comparisons, is the localization of conserved arginine (Arg) 601 to a position in helix 11 identical to amino acids shown to be involved in substrate contact and selection in GlpT and LacY

(27–29). This Arg is conserved across all of the 16 rat sequences and nearly all other known Oatps and is suggestive of a very direct role in substrate transport.

### Subcellular localization of Oatp1c1 mutants

When viewed laterally (*x-y*), wild-type (WT) Oatp1c1 is predominantly localized to the plasma membrane, with a small amount of cytoplasmic expression (Fig. 3A). Oatp1c1 mutants including W277A/W278A, W277F/W278F, G399A/G409A, and G399V/G409V displayed plasma membrane localization similar to WT (Fig. 3, C–F). P609A and R601S also displayed plasma membrane localization; however, some expressed protein was also localized within the cell in perinuclear regions (Fig. 3, H and G). Intracellular trapping was significantly greater for P609A. Mutations of the polar conserved amino acids in TMD 2, including D85A, E89A, and N92A showed no plasma membrane staining, with all observed expression occurring in perinuclear regions and punctate cytoplasmic deposits (Fig. 3, I–K), suggestive of Oatp1c1 trapping within the endoplasmic reticulum.

### Screen for mutant Oatp1c1 T<sub>4</sub> transport activity

Mutants were next screened for T<sub>4</sub> transport activity in an *in vitro* uptake assay. Cells were transiently transfected and then assessed for uptake of 1 nM <sup>125</sup>I-T<sub>4</sub> during a 10-min incubation (Fig. 4). As expected, mutations in TMD 2 that resulted in intracellular trapping including D85A, E89A, and N92A showed no transport activity above empty vector-transfected cells. The conservative W277F/F278F mutation in TMD 5 retained WT T<sub>4</sub> transport activity, but the less conservative W277A/W278A mutation reduced T<sub>4</sub> uptake to empty vector levels. In TMD 8, G399A/G409A and G399V/G409V mutants displayed near WT Oatp1c1 activity at 81 and 77% of control, respectively. TMD 11 R601S and P609A mutants resulted in attenuated T<sub>4</sub> transport compared with WT Oatp1c1; however, transport was still significantly greater than empty vector uptake. At 10 min, R601S uptake was 56% of WT control, whereas P609A was 58% of WT control.

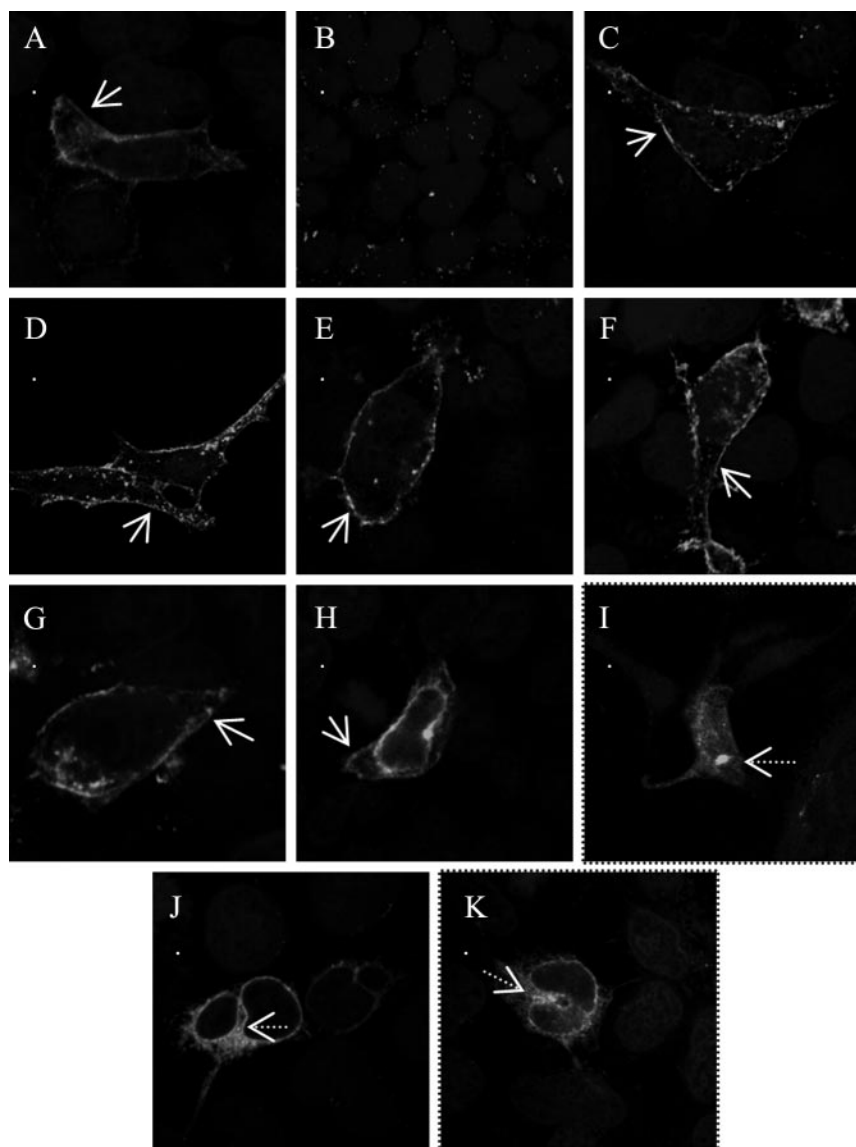


**FIG. 3.** Subcellular localization of Oatp1c1 mutants using immunofluorescence. V5 primary and fluorescein isothiocyanate-conjugated secondary antibodies were used to probe for expression of V5-tagged Oatp1c1 wild-type and mutant constructs (A–K). WT Oatp1c1 (A) displayed plasma membrane staining (*arrow*), whereas empty pEF-DEST51 transfected cells showed only background staining (B). Oatp1c1 mutants W277A,W278A (C), W277F,W278F (D), G399A,G409A (E), and G399V, G409V (F) displayed predominantly plasma membrane staining expression patterns as indicated by *arrows*. Oatp1c1 mutants R601S (G) and P609A (H) displayed plasma membrane staining (*arrows*) with some cytoplasmic localization. Oatp1c1 mutants D85A (I), E89A (J), and N92A (K) displayed only cytoplasmic expression (*dashed arrows*).

### Kinetic characterization of Oatp1c1 mutants

The four mutants that displayed no  $T_4$  transport activity above empty vector transfected cells, including D85A, E89A, N92A, and W277A/W278A were not further characterized. The kinetic characteristics of the remaining mutants were assessed with detailed  $T_4$  uptake time course and velocity *vs.* substrate concentration assays.

WT Oatp1c1 transiently transfected into HEK293 cells resulted in time-dependent accumulation of  $^{125}\text{I}-T_4$  at 37°C. Uptake of 1 nM  $^{125}\text{I}-T_4$  increased linearly for the first 7.5

min and remained at equilibrium thereafter (Fig. 5A). Kinetic parameters were then assessed at 4-min time points over a wide range of  $T_4$  concentrations (0.1–400 nM). Similar to observations in Oatp1c1 stably transfected HEK293 cells (8), HEK293 cells transiently transfected with WT Oatp1c1 demonstrated multisite, biphasic transport kinetics (Fig. 5B). Uptake was best fit with a biphasic nonlinear regression equation ( $R^2 = 0.98$ ), resulting in a high-affinity binding site Michaelis constant ( $K_m$ )<sub>1</sub> of 2.0 nM. In support of biphasic Oatp1c1  $T_4$  transport, when the data were replotted in the form of an Eadie-Hofstee plot, a two-phase profile resulted (Fig. 5C).

W277F/W278F Oatp1c1 transported 1 nM  $^{125}\text{I}-T_4$  with a magnitude and time dependency similar to WT. Uptake was linear until approximately 7.5 min and then remained at equilibrium at subsequent time points (Fig. 5D). The W277F/W278F amino acid substitutions appeared to have a slight effect on the  $T_4$  concentration dependence of Oatp1c1 transport, slightly attenuating the discrete break point at approximately 50 nM between initial rapid increase in velocities and the slow rise at higher concentrations thereafter. Nonetheless,  $T_4$  uptake was best fit with biphasic equation ( $R^2 = 0.98$ ), resulting in a high-affinity  $K_{m1}$  of 22 nM (Fig. 5E). The two-phase profile of Eadie-Hofstee plot was also not as distinct as that observed with WT Oatp1c1, but a break from linearity occurred at higher velocities (Fig. 5F).

In  $^{125}\text{I}-T_4$  uptake time courses, the Oatp1c1 double-glycine mutants G399A/G409A and G399V/G409V transported with similar characteristics to WT Oatp1c1. For G399A/G409A,  $T_4$  uptake was linear for the first 10 min and then reached equilibrium (Fig. 5G). G399V/G409V exhibited linear  $^{125}\text{I}-T_4$  uptake for at least the first 5 min and reached equilibrium at 10 min (Fig. 5J). For both mutants the dynamic range of substrate uptake (signal above empty vector) was similar to that of WT Oatp1c1. However, G399A/G409A and G399V/G409V concentration-dependent transport kinetics varied dramatically

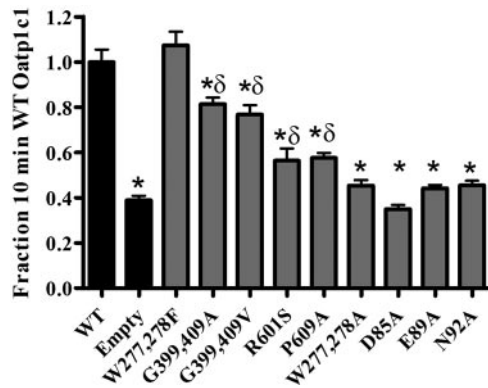


**FIG. 4.**  $T_4$  transport screen. Uptake of 1 nM  $^{125}\text{I}$ - $T_4$  was examined at 10-min time points in cells transiently transfected with WT Oatp1c1, empty vector pEF-DEST 51, and W277A,W278A, W277F,W278F, G399A,G409A, G399V,G409V, R601S, P609A, D85A, E89A, and N92A Oatp1c1 mutants. Data are presented as fraction of WT Oatp1c1  $^{125}\text{I}$ - $T_4$  uptake at 10 min at 37 C. \*, Statistical difference ( $P < 0.05$ ) compared with WT uptake as determined by ANOVA with a Bonferroni *post hoc* test (GraphPad Prism).  $\delta$ , Statistical difference ( $P < 0.05$ ) compared with empty vector uptake as determined by ANOVA with a Bonferroni *post hoc* test (GraphPad Prism). Each point represents the mean uptake  $\pm$  SE ( $n = 3$ ).

from WT Oatp1c1 (Fig. 5, H and K, respectively). Initial velocities rapidly increased in a linear fashion at low  $T_4$  concentrations, but at  $T_4$  concentrations greater than 100 nM, velocities decreased. Because of the unique data patterns, velocity *vs.* substrate data were not fit and a  $K_m$  for  $T_4$  transport was not calculated for either mutant. However, the decrease in velocities at high  $T_4$  concentrations suggests an apparent case of substrate inhibition or perhaps a protein conformational transition as substrate begins to occupy the low-affinity  $T_4$  binding site. Eadie-Hofstee plots for both G399A/G409A and G399V/G409V did not yield a profile characteristic of substrate inhibition (Fig. 5, I and L, respectively).

R601S Oatp1c1 transported  $^{125}\text{I}$ - $T_4$  in a linear fashion for 5 min and then reached equilibrium at approximately 10 min (Fig. 5M). However, the  $^{125}\text{I}$ - $T_4$  uptake dynamic range between R601S and empty vector was greatly reduced compared with WT Oatp1c1. In velocity *vs.* substrate assays, smaller initial velocity increases at low  $T_4$  concentrations (Fig. 5N) produced a more shallow hyperbolic uptake profile instead of the biphasic profile observed with WT Oatp1c1 (Fig. 5B). However, an Eadie-Hofstee displayed a biphasic profile with a sharp division between two transport phases, supportive of at least partial activity in multiple sites (Fig. 5O). Informed by the biphasic Eadie-Hofstee plot, R601S transport data were fit with a biphasic equation, resulting in a  $K_{m1}$  of 32 nM.

Finally, P609A-mediated uptake of 1 nM  $^{125}\text{I}$ - $T_4$  increased linearly for the first 5 min and reached at equilibrium at approximately 10 min (Fig. 5P). Similar to

R601S, the dynamic range between P609A and empty vector-transfected cells was reduced. The velocity *vs.* substrate concentration data were suggestive of biphasic uptake, but velocities were reduced and high-affinity  $K_{m1}$  was increased (42 nM) compared with WT (Fig. 5Q). Eadie-Hofstee plots also displayed a biphasic profile (Fig. 5R). Kinetic parameters for all Oatp1c1 constructs are summarized in Table 1.

## Discussion

In the present study, we sought to develop two- and three-dimensional predictive models to identify and characterize Oatp1c1 amino acids responsible for the specificity filter used in substrate recognition/discrimination and transport. An Oatp1c1 membrane consensus topology map was generated (Fig. 1). Comparison of all 16 rat Oatp amino acid sequences showed considerable evolutionary conservation despite unique tissue distributions and substrate preferences. The level of conservation varied between the 12 predicted TMDs (Fig. 1). TMD 2 displayed the highest level of conservation followed by TMDs 3, 6, and 11. Conserved and invariable amino acids within the TMDs consisted of both structural amino acids such as glycines and prolines and potentially functional amino acids including lysines, arginines, aspartates, and glutamates. The conserved amino acids identified likely contribute to the substrate channel selectivity, translocation mechanism, and/or structural stabilization common to all rat Oatps and perhaps Oatps in general.

We created a three-dimensional model of Oatp1c1 based on the known, high-resolution crystal structures of three MFS transporters, each containing 12 TMDs and displaying a 2-fold symmetry across two sets of six topologically related helices: GlpT, LacY, and EmrD (Fig. 2). The homology model places the majority of conserved and identical amino acids facing the putative substrate channel. Importantly, very few polar and no charged amino acids face the lipid bilayer, a measure of model reliability in TM proteins (Fig. 2, *inset*). Even though sequence homology between rat Oatp1c1 and the three MFS transporters is relatively low (6–9% identity and 22–28% similarity), there was high coincidence between the newly generated TMDs of the Oatp1c1 homology model and the predicted rat Oatp1c1 TMDs in the membrane topology. Importantly, the location of many conserved amino acids in the putative substrate channel coincide with analogous amino acids involved in substrate binding and transport in the extensively studied GlpT and LacY transporters. We discuss specific examples below. These observations support an evolutionary relationship of the Oatps to the prokaryotic 12 transmembrane helix MFS transporters.

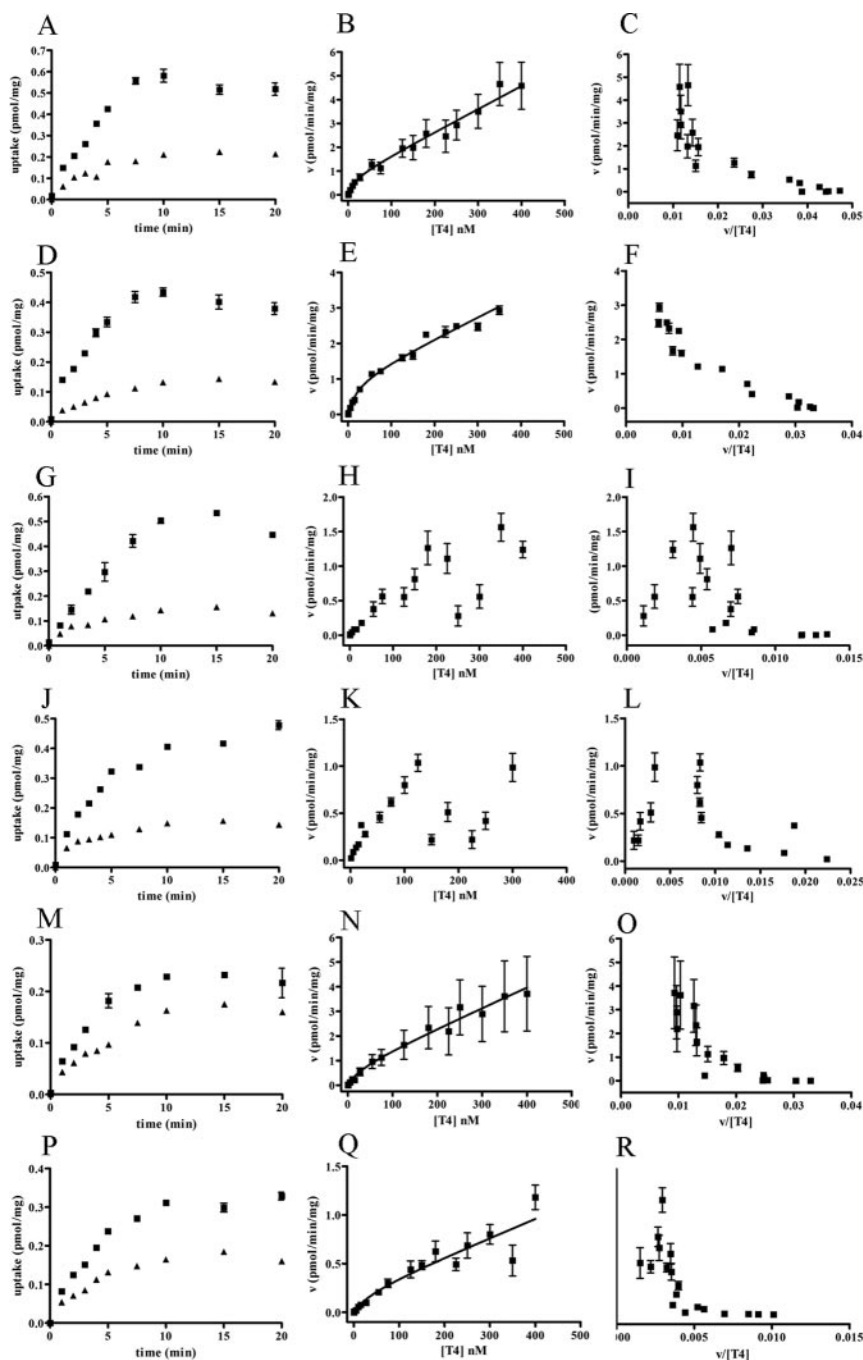


**FIG. 5.** Characterization of mutant Oatp1c1  $T_4$  transport kinetics.  $T_4$  transport kinetics in the form of time courses (*left column*), velocity vs. substrate concentration (*middle column*), and Eadie Hofstee plots (*right column*) were performed in transiently transfected HEK293 cells for WT Oatp1c1 (A–C), W277F,W278F (D–F), G399A, G409A (G–I), G399V, G409V (J–L), R601S (M–O), and P609A (P–R). For time courses (*left column*), uptake of  $^{125}I$ - $T_4$  was monitored at multiple time points in HEK293 cells transiently transfected with either Oatp1c1 construct (*square*) or empty pEF-DEST 51 (*triangle*). For velocity vs. substrate concentration experiments, uptake of varying concentrations of  $T_4$  was examined at 4 min at 37 C, except for Oatp1c1 R601S and P609A, which were monitored at 4.50-min time points. For time courses, each *point* represents the mean uptake minus empty vector zero minute uptake  $\pm$  SE ( $n = 3$ ). For velocity vs. substrate concentration experiments, each *point* represents the mean Oatp1c1 construct uptake minus empty vector contributions at equivalent time points and substrate concentrations  $\pm$  SE ( $n = 3$ ). All kinetic experiments were conducted at least two times with similar results obtained.

Several lines of evidence exist suggesting the presence of multiple binding sites within Oatps. This property is not unique to Oatp/OATP transporters. Additional multispecific transporters are known to possess multiple substrate binding sites including P-glycoprotein or permeability glycoprotein and multidrug resistance protein 1 (30, 31). Interestingly, these transporters also accept many of the same substrates as Oatps/OATPs, including  $T_4$  and  $\beta$ -estradiol 17- $\beta$ -D-glucuronide, suggesting there may be common structural motifs involved. Importantly, several evolutionarily distant prokaryotic MFS transporters have been shown experimentally to have multiple substrate binding sites (32–34). Our previous work has demonstrated the presence of high- and low-affinity binding sites in Oatp1c1 involved in the transport of two substrates,  $T_4$  and  $\beta$ -estradiol 17- $\beta$ -D-glucuronide (8). The multiple binding sites lead to the observed biphasic transport kinetics for WT Oatp1c1 and most mutant forms.

Based on evolutionary conservation, localization to TMDs, orientation within the putative pore, and chemical character of the specific side chains, we analyzed the contribution of residues D85, E89, N92, W277/W278, G399/G409, R601, and P609 to Oatp1c1 structure/function. As observed in Figs. 3A and 5, A–C, WT rat Oatp1c1 was expressed at the plasma membrane and displayed biphasic uptake of  $T_4$ , suggestive of multiple binding sites. All Oatp1c1 mutations appeared to have some degree of effect on either subcellular localization or  $T_4$  transport kinetics (Figs. 3–5 and Table 1). In TMD 2, the most highly conserved helix, mutation of D85, E89, or N92 to alanine caused intracellular trapping of Oatp1c1 (Fig. 3, I–K) and no  $T_4$  transport activity (Fig. 4). The lack of cell surface expression suggests that these residues, at the very least, are involved in the structural integrity of Oatp1c1. In the Oatp1c1 model TMD 2 is adjacent to TMD 11, across the 2-fold

**TABLE 1.** T<sub>4</sub> affinity of Oatp1c1 WT and mutant forms

Oatp1c1 construct	High affinity K <sub>m1</sub>
WT	2 nM
W277F, W278F	22 nM
R601S	32 nM
P609A	42 nM
G399A, G409A	n/a
G399V, G409V	n/a

n/a, Not applicable.

symmetry axis, and may be involved in a network of interactions including providing a counter change to conserved amino acid R601 (see below) or other Lys/Arg residues in the substrate channel. In the current model, Oatp1c1 is in an intracellular open/extracellular closed state (inward facing conformation). In this state D85 and E89 appear to be stabilizing the outward closed state by salt links.

Conserved Oatp1c1 amino acids W277 and W278, capping the N-terminal end of TMD 6, were shown to be important in T<sub>4</sub> transport. When conservatively commutated to similar bulky aromatic phenylalanines, W277F/W278F displayed near WT transport activity in both time course and velocity *vs.* substrate concentration assays (Fig. 5, D–F). In addition, the biphasic profile observed in WT Oatp1c1 was largely maintained. In contrast, when W277 and W278 were replaced with alanines, Oatp1c1 transport activity was abolished (Fig. 4). Based on these data, W277 and W278 likely provide required steric constraints critical at the interface between the Oatp1c1 extracellular domain and substrate pore. These steric constraints were likely partially substituted by the bulk of the phenylalanines but not by the much smaller alanines. It is unclear whether these steric restraints are directly involved in substrate binding/selection or more generally in helix packing or orientation. The WW sequence is part of a larger signature sequence of all Oatps, D-X-R-W-(I/V)-G-A-W-W-X-G-(F/L)-L, the function of which is not known (35).

Conserved glycines in TMD 8 are also important in Oatp1c1 transport kinetics (Fig. 5, G–I and J–L). Transport velocities were greatly reduced at intermediate and high T<sub>4</sub> concentrations with both G399A/G409A and G399V/G409V mutations (Fig. 5, H and K). The high entropic cost associated with inserting glycines into a transmembrane helix and the high evolutionary conservation of G399 and G409 suggest that these residues are critically important for proper Oatp function. The lack of side-chain volume may be important in helix-helix packing for proper channel formation or potentially contribute to a flexible switch alternating between input and output states. Observation of glycines and prolines in transmem-

brane helices has been suggested to be important for the mechanism of receptors, ion channels, and transporters (36–38). In the case of Oatp, a rocker-switch mechanism analogous to the prokaryotic MFS transporters is likely involved. The lack of large effects on T<sub>4</sub> transport at low T<sub>4</sub> concentrations suggests that the low-affinity Oatp1c1 T<sub>4</sub> binding site is affected to a greater degree by these mutations. However, at T<sub>4</sub> concentrations predicted to engage the low-affinity site, binding at the high-affinity site appears to be influenced as well (Fig. 5, H and K). This is suggestive of substrate inhibition, perhaps as a result of nonproductive binding of the low-affinity binding site or possibly a collapse in the input/output switch as the low affinity site becomes engaged only to be thermodynamically overcome at very high substrate concentrations via substrate driven protein stabilization.

R601 in TMD 11 is very highly conserved across all Oatps. In fact, across 12 human, 16 rat, 19 mouse, and nine zebrafish Oatp sequences only Arg or Lys was observed at this position. We mutated R601 based on this conservation, location in the Oatp1c1 model and Oatp preference for anionic substrates. R601S displayed partial T<sub>4</sub> transport activity compared with WT (Fig. 4) and retained an overall biphasic profile (Fig. 5, N and O). However, as seen in Table 1, the high-affinity K<sub>m1</sub> value (32 nM) was increased compared with WT (2 nM). Canonical Oatp/OATP substrates contain a hydrophobic center, a hydrogen bond donor on one end, and negative charge on the opposite end (39). The R601 residue may serve as a countercharge for anionic binding to Oatp1c1 and may explain the reduced T<sub>4</sub> transport capabilities in the R601S mutant. Importantly, in our current model, the position of Arg601 coincides with Y393, recently proposed to be involved in substrate discrimination by molecular dynamics and mutagenesis studies for bacterial MFS member GlpT (29). Furthermore, the identical position in LacY, K358, has been suggested to be involved in hydrogen bonding to substrate (28). It is possible that other charged residues within the TMDs also assist in providing a substrate counter charge. Four positively charged lysines are distributed in TMDs 1, 5, and 9. In support of there being some flexibility in absolute placement of transmembrane side chains, mutational analysis of a conserved Arg in TMD 2 of a *Aspergillus nidulans* nitrate transporter leading to growth arrest was recovered by a second-site revertant N459K in adjacent TMD 11, analogous to the position of R601 (40). The lack of an even stronger effect of R601S on K<sub>m</sub> can be explained by the fact that Oatp/OATP transport can proceed without the presence of a positive counter charge as some neutral and positively charged substrates have been identified (35). Our data suggest R601 may increase binding affinity and/or selec-

tivity but is not absolutely required for Oatp/OATP substrate transport.

Finally, P609A displayed partial T<sub>4</sub> transport activity (Fig. 4). However, significant intracellular trapping of P609A was observed compared with WT Oatp1c1 (Fig. 3H). P609 may introduce helical constraints by generating a kink or break in the  $\alpha$ -helix, perhaps allowing or orienting the different surfaces of the helix to face the substrate pore. D’Rozario and Sansom (41) showed, through molecular dynamics simulation, that transmembrane helices of GlpT containing prolines were significantly more flexible than helices not containing prolines. They suggested that this unique flexibility may be required for the rocker-switch mechanism proposed for GlpT and other MFS members. The conservation and location of glycines and prolines in Oatps appears consistent with this result. The 20-fold increase in the K<sub>m</sub> value shows that P609 plays a role in T<sub>4</sub> binding. Presumably this change in K<sub>m</sub> is the result of subtle changes in helix packing and/or orientation but may also arise from altered inward- and outward-facing interconversion in a rocker-switch mechanism. The significant intracellular trapping suggests that P609 may also be playing a role in proper Oatp1c1 folding.

In the current study, in addition to gaining basic information about amino acids involved in creating the general specificity filter for Oatp1c1 substrate recognition, we sought to identify specific amino acids that define the discrete binding sites. Based on our expression, initial screen for transport activity, and structural *vs.* functional mutation, the only amino acids in our group of mutations having direct effects on one binding site or the other were W277F/W278F and R601S. Concentration-dependent T<sub>4</sub> uptake suggested the high-affinity T<sub>4</sub> binding site was primarily affected with little change in the low-affinity slope. This suggests that these residues may be directly involved in substrate recognition at the high-affinity site. Evaluating the transport capabilities of functional Oatp1c1 mutants using substrates other than T<sub>4</sub> may reveal more about the substrate binding site organization and the complementarity of Oatp1c1 substrate surfaces.

Most of the current data on mutational effects in Oatps/OATPs come from pharmacogenetic studies on naturally occurring polymorphic OATPs (42, 43). A recent paper by van der Deure *et al.* (44) found an association between noncoding OATP1C1-intron3C>T and OATP1C1-C3035T polymorphisms and low scores on psychological well-being tests in adequately treated hypothyroid patients. However, in a subsequent study, no differences in *in vitro* thyroid hormone transport or serum thyroid hormone levels between noncoding and coding (OATP1C1-Pro143Thr) polymorphisms and WT OATP1C1 were measured (45). These results are

consistent with our rat Oatp1c1 topology and three-dimensional models placing OATP1C1-Pro143 in a poorly conserved loop between TMDs 3 and 4, suggesting no direct role in substrate selectivity or transport.

A limited number of modeling and mutagenesis studies have also been carried out on the Oatps. The 10 invariable cysteines between helices 9 and 10, characteristic of all Oatps, were shown to be required for OATP2B1 function and displayed misprocessing (46). Meier-Abt *et al.* (10) generated homology models for OATP1B3 and OATP2B1 identifying positive electrostatic potential in the resulting pore and a unique location of conserved glycines and prolines in the transmembrane helices. The location of these residues was suggested to orient important residues in TMDs 8 and 10 toward the substrate channel, one proline identified was equivalent to P609 above. Gui and Hagenbuch (47) generated a model of OATP1B3 and used the model and sequence comparison to generate OATP1B3/1B1 chimeric and OATP1B3 TMD 10 mutant proteins. Their results suggest that TMD 10 residues, specifically Y537, S545, and T550, make direct contact with substrate, cholecystokinin octapeptide. More recent studies on paralog OATP1B1 concur with the critical nature of TMD 10 in transport (48). Our model, described above, also places these critical amino acids facing the substrate channel 10–20 Å (depending on Arg side chain rotamer) from the conserved R601.

In conclusion we have predicted and characterized amino acids involved with maintenance of Oatp1c1 structural integrity and T<sub>4</sub> transport function. We have established a strong evolutionary relationship between the Oatps and MFS transporters, including structural and mechanistic similarities, in support of our proposed Oatp1c1 model. By making this association, we have made available the wealth of knowledge of MFS structure/function in understanding Oatp transport. An understanding of Oatp structure and function will help elucidate their biological role and significance at tissue barriers. Future structure/function studies along with comparative molecular field analysis of substrates will allow the mapping of complementary Oatp1c1 and substrate surfaces, with the ultimate goal of identifying novel Oatp1c1 endo- and xenobiotic substrates trafficked at the blood-brain barrier and perhaps the design of Oatp modifiers/inhibitors.

## Acknowledgments

We acknowledge Gregg Baldeshwiler and Becca Bartley for their technical assistance. Technical assistance was provided by the University of Minnesota Brain Barriers Research Center.

Address all correspondence and requests for reprints to: Jon N. Rumbley, Ph.D., Department of Pharmacy Practice and Pharmaceutical Sciences, 232 Life Science, 1110 Kirby Drive, University of Minnesota-Duluth, Duluth, Minnesota 55812. E-mail: jrumbley@d.umn.edu.

This work was supported by Research Corporation Grant CC6681 (to J.N.R.); the University of Minnesota Graduate School (to G.W.A.); and a Torske Klubben fellowship (to D.E.W.).

Disclosure Summary: The authors have nothing to disclose.

## References

- Hagenbuch B, Meier PJ 2003 The superfamily of organic anion transporting polypeptides. *Biochim Biophys Acta* 1609:1–18
- Mikkaichi T, Suzuki T, Tanemoto M, Ito S, Abe T 2004 The organic anion transporter (OATP) family. *Drug Metab Pharmacokinet* 19: 171–179
- Roberts LM, Woodford K, Zhou M, Black DS, Haggerty JE, Tate EH, Grindstaff KK, Mengesha W, Raman C, Zerangue N 2008 Expression of the thyroid hormone transporters monocarboxylate transporter-8 (SLC16A2) and organic ion transporter-14 (SLCO1C1) at the blood-brain barrier. *Endocrinology* 149: 6251–6261
- Sugiyama D, Kusuhara H, Taniguchi H, Ishikawa S, Nozaki Y, Aburatani H, Sugiyama Y 2003 Functional characterization of rat brain-specific organic anion transporter (Oatp14) at the blood-brain barrier: high affinity transporter for thyroxine. *J Biol Chem* 278: 43489–43495
- Tohyama K, Kusuhara H, Sugiyama Y 2004 Involvement of multispecific organic anion transporter, Oatp14 (Slc21a14), in the transport of thyroxine across the blood-brain barrier. *Endocrinology* 145:4384–4391
- Hagenbuch B 2007 Cellular entry of thyroid hormones by organic anion transporting polypeptides. *Best Pract Res* 21:209–221
- Hagenbuch B, Gui C 2008 Xenobiotic transporters of the human organic anion transporting polypeptides (OATP) family. *Xenobiotica* 38:778–801
- Westholm DE, Salo DR, Viken KJ, Rumbley JN, Anderson GW 2009 The blood-brain barrier thyroxine transporter organic anion-transporting polypeptide 1c1 displays atypical transport kinetics. *Endocrinology* 150:5153–5162
- Abramson J, Smirnova I, Kasho V, Verner G, Kaback HR, Iwata S 2003 Structure and mechanism of the lactose permease of *Escherichia coli*. *Science (New York, NY)* 301:610–615
- Meier-Abt F, Mokrab Y, Mizuguchi K 2005 Organic anion transporting polypeptides of the OATP/SLCO superfamily: identification of new members in nonmammalian species, comparative modeling and a potential transport mode. *J Membr Biol* 208:213–227
- Huang Y, Lemieux MJ, Song J, Auer M, Wang DN 2003 Structure and mechanism of the glycerol-3-phosphate transporter from *Escherichia coli*. *Science (New York, NY)* 301:616–620
- Yin Y, He X, Szcwycyk P, Nguyen T, Chang G 2006 Structure of the multidrug transporter EmrD from *Escherichia coli*. *Science (New York, NY)* 312:741–744
- Westholm DE, Stenhejm DD, Rumbley JN, Drewes LR, Anderson GW 2009 Competitive inhibition of organic anion transporting polypeptide 1c1-mediated thyroxine transport by the fenamate class of nonsteroidal antiinflammatory drugs. *Endocrinology* 150:1025–1032
- Pei J, Grishin NV 2007 PROMALS: towards accurate multiple sequence alignments of distantly related proteins. *Bioinformatics (Oxford, England)* 23:802–808
- Juretić D, Zoranić L, Zucić D 2002 Basic charge clusters and predictions of membrane protein topology. *J Chem Inf Comput Sci* 42:620–632
- Cserzo M, Eisenhaber F, Eisenhaber B, Simon I 2004 TM or not TM: transmembrane protein prediction with low false positive rate using DAS-TMfilter. *Bioinformatics (Oxford, England)* 20:136–137
- Taylor PD, Attwood TK, Flower DR 2003 BPROMPT: a consensus server for membrane protein prediction. *Nucleic Acids Res* 31:3698–3700
- Jones DT 2007 Improving the accuracy of transmembrane protein topology prediction using evolutionary information. *Bioinformatics (Oxford, England)* 23:538–544
- Tusnády GE, Simon I 2001 The HMMTOP transmembrane topology prediction server. *Bioinformatics (Oxford, England)* 17:849–850
- Bagos PG, Liakopoulos TD, Hamodrakas SJ 2006 Algorithms for incorporating prior topological information in HMMs: application to transmembrane proteins. *BMC Bioinformatics* 7:189
- Käll L, Krogh A, Sonnhammer EL 2004 A combined transmembrane topology and signal peptide prediction method. *J Mol Biol* 338: 1027–1036
- Käll L, Krogh A, Sonnhammer EL 2005 An HMM posterior decoder for sequence feature prediction that includes homology information. *Bioinformatics (Oxford, England)* 21(Suppl 1):i251–i257
- Beitz E 2000 T(E)Xtopo: shaded membrane protein topology plots in LAT(E)X2epsilon. *Bioinformatics (Oxford, England)* 16:1050–1051
- Sali A, Blundell TL 1993 Comparative protein modelling by satisfaction of spatial restraints. *J Mol Biol* 234:779–815
- Pei J, Kim BH, Grishin NV 2008 PROMALS3D: a tool for multiple protein sequence and structure alignments. *Nucleic Acids Res* 36: 2295–2300
- Pettersen EF, Goddard TD, Huang CC, Couch GS, Greenblatt DM, Meng EC, Ferrin TE 2004 UCSF Chimera—a visualization system for exploratory research and analysis. *J Comput Chem* 25:1605–1612
- Jensen MØ, Yin Y, Tajkhorshid E, Schulten K 2007 Sugar transport across lactose permease probed by steered molecular dynamics. *Biophys J* 93:92–102
- Klauda JB, Brooks BR 2007 Sugar binding in lactose permease: anomeric state of a disaccharide influences binding structure. *J Mol Biol* 367:1523–1534
- Law CJ, Enkavi G, Wang DN, Tajkhorshid E 2009 Structural basis of substrate selectivity in the glycerol-3-phosphate: phosphate antiporter GlpT. *Biophys J* 97:1346–1353
- Karwatsky JM, Georges E 2004 Drug binding domains of MRP1 (ABCC1) as revealed by photoaffinity labeling. *Curr Med Chem* 4:19–30
- Aller SG, Yu J, Ward A, Weng Y, Chittaboina S, Zhuo R, Harrell PM, Trinh YT, Zhang Q, Urbatsch IL, Chang G 2009 Structure of P-glycoprotein reveals a molecular basis for poly-specific drug binding. *Science (New York, NY)* 323:1718–1722
- Lewinson O, Bibi E 2001 Evidence for simultaneous binding of dissimilar multidrug substrates by the *Escherichia coli* multidrug transporter MdfA. *Biochemistry* 40:12612–12618
- Mitchell BA, Paulsen IT, Brown MH, Skurray RA 1999 Bioenergetics of the staphylococcal multidrug export protein QacA. Identification of distinct binding sites for monovalent and divalent cations. *J Biol Chem* 274:3541–3548
- Putnam M, Koole LA, van Veen HW, Konings WN 1999 The secondary multidrug transporter LmrP contains multiple drug interaction sites. *Biochemistry* 38:13900–13905
- Hagenbuch B, Meier PJ 2004 Organic anion transporting polypeptides of the OATP/SLC21 family: phylogenetic classification as OATP/SLCO superfamily, new nomenclature and molecular/functional properties. *Pflugers Arch* 447:653–665
- Beckstein O, Biggin PC, Bond P, Bright JN, Domene C, Grottesi A, Holyoake J, Sansom MS 2003 Ion channel gating: insights via molecular simulations. *FEBS Lett* 555:85–90

37. De Jesus M, Jin J, Guffanti AA, Krulwich TA 2005 Importance of the GP dipeptide of the antiporter motif and other membrane-embedded proline and glycine residues in tetracycline efflux protein Tet(L). *Biochemistry* 44:12896–12904
38. Sansom MS, Weinstein H 2000 Hinges, swivels and switches: the role of prolines in signalling via transmembrane  $\alpha$ -helices. *Trends Pharmacol Sci* 21:445–451
39. Yarim M, Moro S, Huber R, Meier PJ, Kaseda C, Kashima T, Hagenbuch B, Folkers G 2005 Application of QSAR analysis to organic anion transporting polypeptide 1a5 (Oatp1a5) substrates. *Bioorg Med Chem* 13:463–471
40. Unkles SE, Rouch DA, Wang Y, Siddiqi MY, Glass AD, Kinghorn JR 2004 Two perfectly conserved arginine residues are required for substrate binding in a high-affinity nitrate transporter. *Proc Natl Acad Sci USA* 101:17549–17554
41. D’Rozario RS, Sansom MS 2008 Helix dynamics in a membrane transport protein: comparative simulations of the glycerol-3-phosphate transporter and its constituent helices. *Mol Membr Biol* 25: 571–583
42. König J, Seithel A, Gradhand U, Fromm MF 2006 Pharmacogenomics of human OATP transporters. *Naunyn Schmiedebergs Arch Pharmacol* 372:432–443
43. Marzolini C, Tirone RG, Kim RB 2004 Pharmacogenomics of the OATP and OAT families. *Pharmacogenomics* 5:273–282
44. van der Deure WM, Appelhof BC, Peeters RP, Wiersinga WM, Wekking EM, Huyser J, Schene AH, Tijssen JG, Hoogendijk WJ, Visser TJ, Fliers E 2008 Polymorphisms in the brain-specific thyroid hormone transporter OATP1C1 are associated with fatigue and depression in hypothyroid patients. *Clin Endocrinol (Oxf)* 69:804–811
45. van der Deure WM, Hansen PS, Peeters RP, Kyvik KO, Friesema EC, Hegedüs L, Visser TJ 2008 Thyroid hormone transport and metabolism by organic anion transporter 1C1 and consequences of genetic variation. *Endocrinology* 149:5307–5314
46. Hänggi E, Grundschober AF, Leuthold S, Meier PJ, St-Pierre MV 2006 Functional analysis of the extracellular cysteine residues in the human organic anion transporting polypeptide, OATP2B1. *Mol Pharmacol* 70:806–817
47. Gui C, Hagenbuch B 2008 Amino acid residues in transmembrane domain 10 of organic anion transporting polypeptide 1B3 are critical for cholecystokinin octapeptide transport. *Biochemistry* 47:9090–9097
48. Gui C, Hagenbuch B 2009 Role of transmembrane domain 10 for the function of organic anion transporting polypeptide 1B1. *Protein Sci* 18:2298–2306